Journal of Medicinal Chemistry

Article

Identification of the new covalent allosteric binding site of FBPase with disulfiram derivatives toward glucose reduction

Yunyuan Huang, yixiang xu, rongrong song, shuaishuai ni, Jiaqi Liu, Yanhong Xu, Yanliang Ren, Li Rao, Yingjie Wang, Lin Wei, lingling feng, Chen Su, Chao Peng, Jian Li, and Jian Wan

J. Med. Chem., **Just Accepted Manuscript** • DOI: 10.1021/acs.jmedchem.0c00699 • Publication Date (Web): 07 May 2020

Just Accepted

is published by the American Chemical Society. 1155 Sixteenth Street N.W., Washington, DC 20036

Identification of the new covalent allosteric binding site of FBPase with disulfiram derivatives toward glucose reduction

Yunyuan Huang[1, #], Yixiang Xu[2, #], Rongrong Song[1, #], Shuaishuai Ni[3, #], Jiaqi Liu[1], Yanhong Xu[1], Yanliang Ren[1,*], Li Rao[1], Yingjie Wang[4], Lin Wei[1], Lingling Feng[1], Chen Su[5], Chao Peng[5], Jian Li[2, *], Jian Wan[1, *]

[1] Key Laboratory of Pesticide & Chemical Biology (CCNU), Ministry of Education, College of Chemistry, Central China Normal University, Wuhan 430079, China

[2] Shanghai Key Laboratory of New Drug Design, School of Pharmacy, East China University of Science and Technology, Shanghai 200237, China

[3] Cancer Institute, Longhua Hospital, Shanghai University of Traditional Chinese Medicine, Shanghai, 200032, China.

[4] Shenzhen Bay Laboratory, Shenzhen 518055, Guangdong, China

[5] National Facility for Protein Science in Shanghai, Zhangjiang Lab, Shanghai, 201210, China

* Corresponding author:

Address: Key Laboratory of Pesticide & Chemical Biology (CCNU), Ministry of Education, College of Chemistry, Central China Normal University, Wuhan 430079, China; E-mails: renyl@mail.ccnu.edu.cn (Y-L. Ren); jianwan@mail.ccnu.edu.cn (J. Wan); Phone: +86-27-67862022. Fax: +86-27-67862022.

Shanghai Key Laboratory of New Drug Design, School of Pharmacy, East China University of Science and Technology, Shanghai 200237, China; E-mail: jianli@ecust.edu.cn; Phone: +86-21-64252584. Fax: +86-21-64252584.

Keywords: disulfiram derivatives, covalent allosteric mechanism, drug repurposing, fructose 1,6-bisphosphatase

ABSTRACT

Fructose 1,6-bisphosphatase (FBPase) has attracted substantial interest as a target associated with cancer and type 2 diabetes. Herein, we found that disulfiram and its derivatives can potently inhibit FBPase by covalently binding to a new C128 allosteric site distinct from the original C128 site in APO FBPase. Further identification of allosteric inhibition mechanism reveal that the covalent binding of a fragment of **214** will result in the movement of C128 and the dissociation of helix H4 (123-128), which in turn allows S123 to more easily form new hydrogen-bonds with K71 and D74 in helix H3 (69-72), thereby inhibiting FBPase activity. Notably, both disulfiram and **212** might moderately reduce blood glucose output *in vivo*. Therefore, our current findings not only identify a new covalent allosteric site of FBPase, but also establish a structural foundation and provide a promising way for the design of covalent allosteric drugs for glucose reduction.

INTRODUCTION

Fructose-1,6-bisphosphatase (FBPase) acts as an important rate-limiting enzyme central to the gluconeogenic (GNG) pathway and regulates metabolism in dysfunctional cells or tissues, such as hepatocytes,[1] renal carcinoma cells,[2] soft tissue sarcomas,[3] cancer stem cells,[4] natural killer cells[5] and hematopoietic progenitor cells.[6] FBPase inhibitors have been developed as a potential strategy for treating cancer[5] and type 2 diabetes (T2D).[7] Moreover, many efforts have been made to discover inhibitors that bind to the AMP allosteric site of FBPase to treat T2D.[7-9] Among these inhibitors, **MB06322** was tested in a phase II clinical trial for the treatment of T2D.[10] However, it has been suggested that a metabolite (**MB05099**)[11] of **MB06322** (Fig. S1) leads to lactic acidosis in humans. Additionally, a previous study[12, 13] reported that the AMP site was a difficult target due to its high dependence on electrostatic binding interactions, and lack of selectivity relative to other important enzymes involved in anabolic and catabolic pathways. To address this concern, discovering and identifying a novel site that can regulate the catalytic activity of FBPase is of utmost importance.

Recently, the discovery of new allosteric sites and modulators has greatly facilitated the design of new drugs.[14, 15] Discovering drugs that covalently bind target protein residues (e.g., cysteine and serine) has become an indispensable strategy for drug discovery due to the high biological activity, high selectivity and long action time[16, 17] of such compounds. Thus, covalent allosteric modulators, which combine the merits of allosteric and covalent drugs, have recently emerged as a research area that has shown great potential for drug discovery.[14, 18-20] KRAS (G12C) was considered to

be an undruggable target for cancer until the discovery of new covalent allosteric modulators.[21, 22] In the last year, **AMG 510**, a KRAS(G12C) allosteric covalent modulator, was approved for clinical trials.[23, 24] In our previous work,[25] we found that several nitrostyrene derivatives could potently inhibit FBPase by covalently binding to the original C128 site,[25] but the details of their covalent allosteric mechanism remain unclear.

Facing a high risk of failure, high costs, and a long period during the research and development (R&D) of novel antidiabetic agents, drug repurposing has been identified as a faster and more economical strategy. Herein, disulfiram**,** a well-known anti-alcoholism[26] and anticancer drug,[27] and its derivatives (**212**/**214**) were used to clarify the covalent allosteric mechanism of the C128 site. It is found that the disulfiram derivative **214** potently inhibit FBPase activity by covalently binding to a novel allosteric binding site, which is distinct from the original C128 site in APO FBPase[25] and not exploited previously. Furthermore, the covalent allosteric mechanism of this new site has been confirmed by integrating the crystallographic structure of FBPase-C128 modified by **214** (a disulfiram derivative), LC-MS, site-directed mutagenesis and molecular dynamics (MD) simulations. Considering the better FBPase inhibitory activities of disulfiram and **212**, the hypoglycemic efficacies of these two compounds in ICR and *db/db* mice were further evaluated.

RESULTS AND DISCUSSION

The synthesis of compounds 212/214

The synthesis of compounds **212** and **214** are shown in Scheme 1, and the

procedure generally followed previous works.[28] Commercially available thiazole-2-thiol was added to a freshly prepared solution of 4-chlorophenyl hypochlorothioite in anhydrous ethyl ether, and the reaction mixture was stirred for 12 h at room temperature to generate compound **212**. Compound **214** was obtained by the oxidation of benzo[*d*]thiazole-2-thiol and ethanethiol by using DDQ as the oxidizing agent. The synthetic procedures are described in the experimental section.

Scheme 1. Synthesis of compounds **212** and **214**

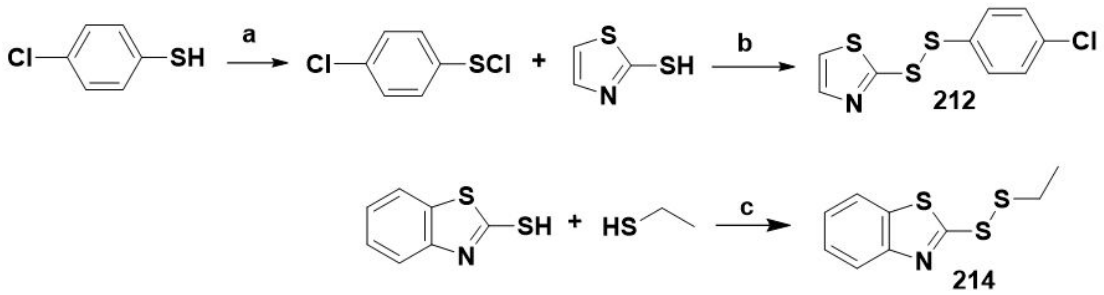

Reagents and conditions: (a)SO_2Cl_2, DCM, 0 °C, 1 h; (b) Et_2O, rt, 12 h; (c) DDQ, DCM, 0 °C, 1 h.

Design of Compounds 212/214.

Targeting cysteine is a practical strategy for discovering covalent inhibitors[17, 29] because of their low occurrence (2.3%) in the human proteome[29] and high selectivity. Thus, several well-established drugs that could covalently modify cysteines were used to explore their alternative functions as novel FBPase inhibitors.[17] Amongst them, disulfiram (Fig. S2) exhibited good biological activity against FBPase (IC_{50}=1.5 μM). The thiazole ring is very common framework in FDA-approved drugs[30] and disulfiram derivatives,[31] Thus, we used a cyclization strategy to further elucidate the inhibitory mechanism of disulfiram and its derivatives (Fig. 1). In addition, the synthesis of asymmetric disulfide derivatives (**212** and **214**) helped us to effectively verify this covalent reaction mechanism. As illustrated in Fig. 1, disulfiram derivatives **212** and

214 also potently inhibited FBPase (IC_{50} = 0.54 μM for **212**, and 1.6 μM for **214**).

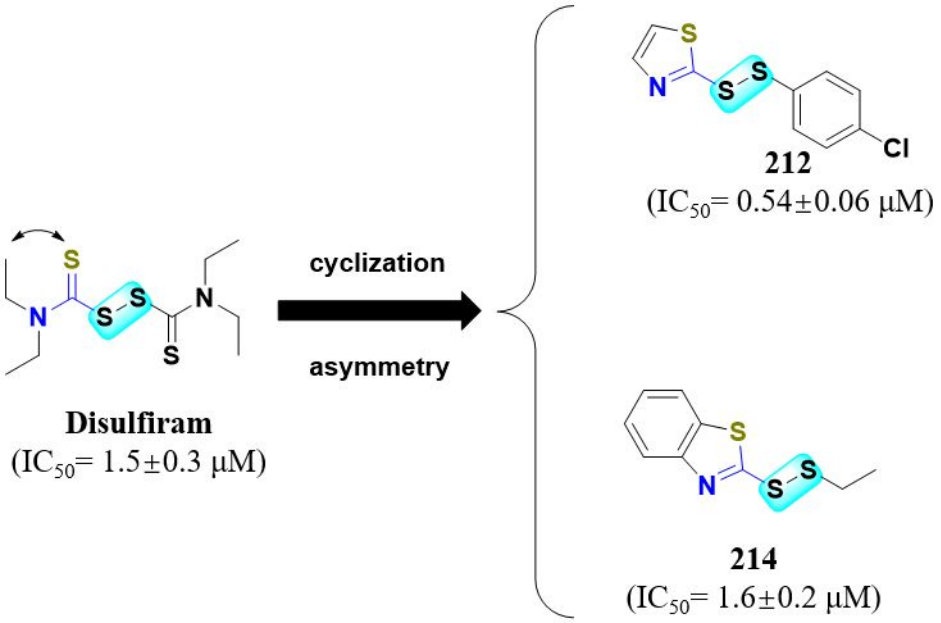

Fig. 1. Designing strategy of asymmetric disulfide compounds **212/214**

Determination and Analysis of FBPase Crystal Structures

To elaborate the allosteric inhibitory mechanism of the disulfiram derivatives, three different FBPase structures (APO PDB:1FTA, FBP-bound PDB:5ZWK, **214b**-bound PDB:6LS5) shown in Fig. 2 were considered. As illustrated in Fig. 2A, S123--I126 (2.9 Å) and N125--C128 (3.0 Å) hydrogen bonds could be observed in the crystal structure of APO FBPase. These two hydrogen-bonds contribute to the formation of the 3_{10}-helix structure, named helix H4. In addition, a new hydrogen-bond between the substrate (FBP) and S123 appeared in the crystal structure of FBP-bound FBPase. Although the hydrogen-bonds of S123--I126 (3.3 Å) and N125--C128 (3.5 Å) could also be observed in the crystal structure of FBP-bound FBPase (Fig. 2B), these two hydrogen-bonds were longer than those in APO FBPase. Moreover, the helical content[32] of H4 in the FBP-bound FBPase structure was decreased compared with that of APO FBPase. Both evidences indicate that the hydrogen-bond between S123 and

FBP could affect the helical content of H4.

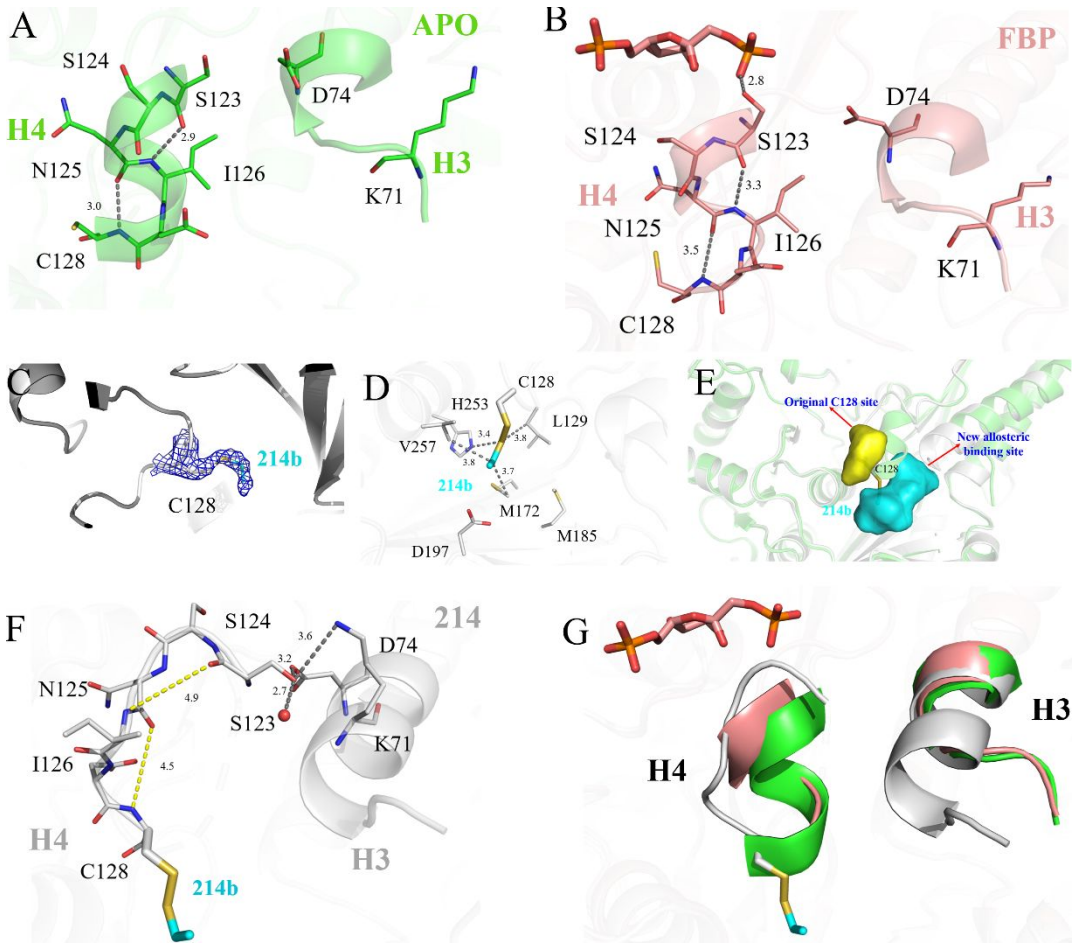

Fig. 2. Crystal Structure of FBPase. (A) Interaction networks between helix H3 (73-88) and helix H4 (123-128) in APO FBPase (PDB: 1FTA, green). (B) Interaction networks between helix H3 and helix H4 in FBP-bound FBPase (PDB: 5ZWK, salmon.) (C) The electron density (2Fo-Fc omit map contoured at 0.8σ) for **214b** bound to C128. (D) Interaction networks between FBPase and **214b**. (E) The pocket variation from original C128 site in APO FBPase/FBP-bound FBPase to new allosteric binding site in **214b**-bound FBPase. (F) Interaction networks between helix H3 and helix H4 in **214b**-bound FBPase (PDB: 6LS5, gray) (G) The conformation comparison between **214b**-FBPase (gray cartoon, PDB ID:6LS5), FBP-bound FBPase (salmon cartoon, PDB ID: 5ZWK) and APO FBPase (green cartoon, PDB ID:1FTA)

The structure of the FBPase cocrystallized with **214b** (a fragment of **214**) was successfully determined at 2.0 Å resolution by X-ray crystallography to identify the allosteric inhibition mechanism of this novel C128-site for the first time. The

crystallographic data are listed in Table 1.

Table 1. Crystallographic data collection and refinement statistics

	Hu-FBPase-**214b** (6LS5)
Data collection[a]	
Space group	$P2_12_12_1$
Wavelength	1.06
Cell dimensions	
a, b, c (Å)	67.44, 83.40, 276.48
α, β, γ (°)	90, 90, 90
Resolution (Å)	42.8-2.03 (2.04-2.03)[b]
R_{merge}	11.5 (63.2)
I/σ (*I*)	11.3 (2.3)
Completeness (%)	99.6 (98.6)
Redundancy	8.1 (7.4)
Refinement	
No.reflections	101,851
R_{work}/R_{free}	19.42/23.73
No.atoms	
Protein	9,909
Ligand/ion	99
Water	640
All Atom	10,648
B-factors	
Protein	32.8
Ligand/ion	41.9
Water	37.5
All Atom	33.1
R.m.s. deviations	
Bond lengths (Å)	0.011
Bond angles (°)	1.119

[a]Data were collected from a single crystal

[b]Values in parentheses are for the highest-resolution shell

A covalent linkage between C128 and **214b** could be observed from the structure of **214b** in complex with FBPase (Fig. 2C). Fig. 2D shows that the C128 pocket for **214b** modification involves residues L129, M172, M185, D197, H253 and V257. As

shown in Fig. 2E, the addition of **214b** to C128 results in the movement of C128 residue and the formation of a new allosteric binding site in **214b**-bound FBPase and the disappearance of the original C128 site [25] in APO FBPase and FBP-bound FBPase. This is most likely to be the driving force for the deactivation of FBPase. Compared with the crystal structures of APO FBPase (Fig. 2A) and FBP-bound FBPase (Fig. 2B), the structure of **214b**-bound FBPase (Fig. 2F) lacks the hydrogen-bonds of S123--FBP, S123--I126 and N125--C128, and helix H4 (Fig. 2F and 2G) was broken. Instead, a new hydrogen-bonding network between S123 and D74, K71 and water was formed. Simultaneously, the helical content of helix H3 in **214b**-bound FBPase was increased compared with those in APO FBPase and FBP-bound FBPase (Fig. 2G).

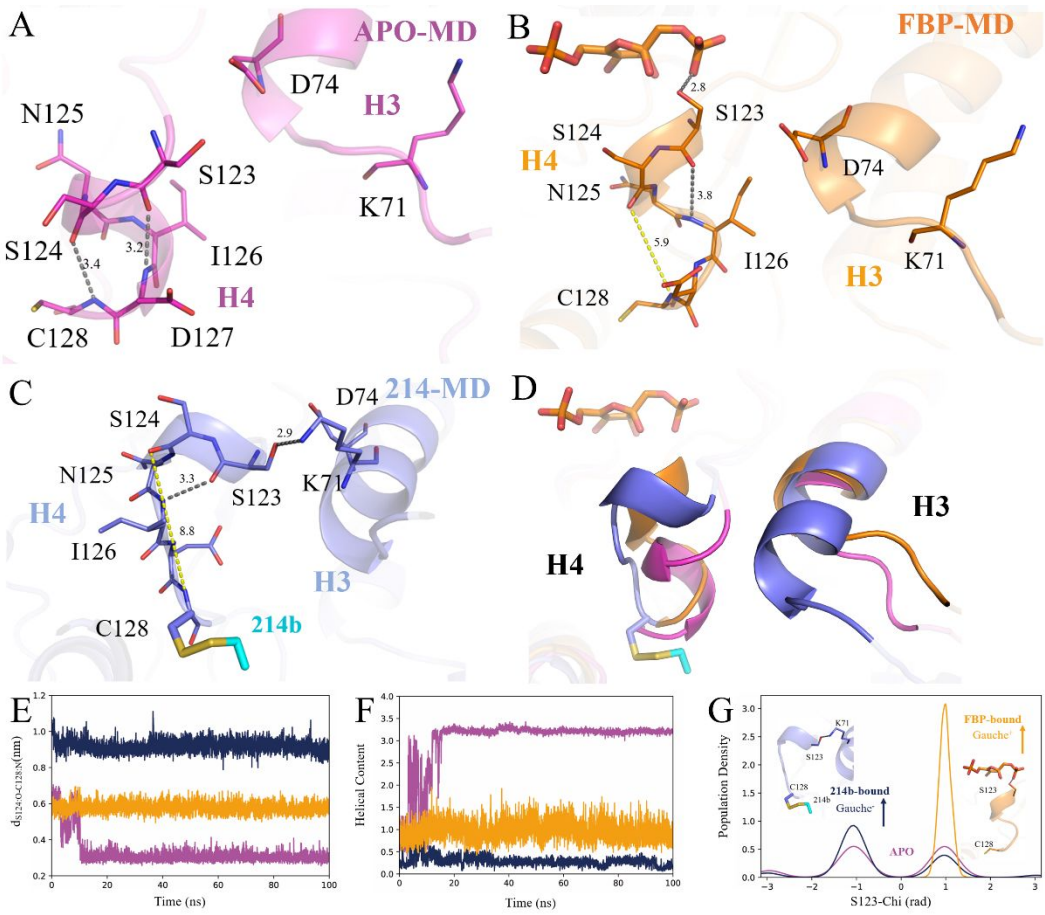

Fig. 3. The analysis of FBPase structures simulated by 100 ns molecular dynamic (MD). (A)

Interaction networks between APO FBPase structure helix H3 and helix H4. (B) Interaction networks between FBP-bound FBPase structure helix H3 and helix H4. (C) Interaction networks between **214b**-bound FBPase structure helix H3 and helix H4. (D) The conformation comparison between **214b**-FBPase (blue cartoon), FBP-bound FBPase (orange cartoon) and APO FBPase (magenta cartoon). (E) Distance change (S124:O-C128:N) of three FBPase structure (APO: magenta line, FBP-bound: orange line, **214b** bound: blue line). (F) Helical content (residue 120-129) change of three FBPase structure (APO: magenta line, FBP-bound: orange line, **214b** bound: blue line). (G) The S123 side chain population density of three FBPase structure (APO: magenta line, FBP-bound: orange line, **214b** bound: blue line) in molecular dynamics balance.

Furthermore, three FBPase structures (APO PDB, FBP-bound and **214b**-bound) were further optimized by MD simulations for 100 ns. As shown in Fig. 3A, the 3_{10}-helix of H4 in the APO FBPase crystal (Fig. 2A) was optimized to form a more stable H4 α-helix by MD simulations (Fig. 3A). The MD structures of FBP-bound FBPase (Fig. 3B) and **214b**-bound FBPase (Fig. 3C) are similar to those in the crystal structure (Fig. 2B and 2F). Notably, there was only one hydrogen-bond between S123 and K71 in the MD structure of **214b**-bound FBPase instead of the hydrogen-bonding network in the **214b**-bound FBPase crystal structure, indicating that the interaction between S123 and K71 was important for the elongation of the new H3 helix (Fig. 3C and 3D). The protein dynamics that contribute to allosteric regulation were further investigated, and plots of the distances (S124:O-C128:N), helical contents (helix H4) and population densities of S123-Chi are illustrated in Fig. 3E, 3F and 3G, respectively. The magenta line represents the helical content of H4, the distance of S124:O-C128:N, and the population density of S123-Chi in APO FBPase, while the orange line represents those in FBP-bound FBPase, and the blue line represents those in **214b**-bound FBPase. As

shown in Fig. 3 (magenta line), in the APO FBPase structure, the S124:O-C128:N distance was approximately 3 Å (Fig 3E), and the helical content was approximately 3.1 (Fig. 3F), both indicating a typical α-helical configuration. Moreover, the population density of S123-Chi in both swing directions (gauche$^-$ and gauche$^+$) was approximately 0.5 (Fig. 3G). However, when FBP was bound to FBPase (Fig. 3 orange line), the helical content (120-129) was decreased to 0.9 and the S124:O-C128:N distance was increased to approximately 6 Å. This indicates that the binding of FBP into FBPase results in the partial dissociation of the 120-129 helix compared with that in APO FBPase. As expected, the swing in/out direction and probability of the S123 side chain (Fig. 3G orange line) show that the S123 side chain in FBP-bound FBPase has an almost gauche$^+$ direction when forming hydrogen-bonds with FBP.

As shown in Fig. 3 (blue line), the S124:O-C128:N distance was increased to approximately 9 Å (Fig. 3E) and the helical content in **214b**-bound FBPase was reduced to approximately 0.3 (Fig. 3F). This demonstrates that the covalent addition of **214b** to C128 results in the dissociation of helix H4 by disrupting the hydrogen-bond between S124 and C128. Based on the above evidence, we inferred that the hydrogen-bond (Fig. 3E) between S124 in position i and C128 in position i+4 significantly contributes to the formation of helix H4 (Fig. 3F). Consistent with our crystal structure of **214**-bound FBPase (Fig. 2F), the addition of **214b** to C128 led to significant repulsion between C128 and the -$CONH_2$ group of N125; thus N125 was far from C128, and the S124-C128 hydrogen-bond was broken, which in turn led to the disruption of helix H4. As expected, the population density of the S123 side chain increases to approximately 1.0

in the gauche$^+$ direction but decreases to approximately 0.3 in the gauche$^-$ direction (Fig. 3G), indicating that most S123 is pointed away from FBP, and forms hydrogen-bonds with K71, D74 and water in helices 69-72 (Fig. 2F gray cartoon). Overall, upon addition of **214b** to C128, N125 is repelled from C128, in turn disrupting the S124-C128 hydrogen-bond and helix H4. Helix H4 is very important for the movement of S123, and the dissociation of helix H4 allows S123 to more easily form a new hydrogen-bond with K71 in elongated helix H3 (69-72). The loss of the S123--FBP hydrogen-bond leads to the inactivity of FBPase. Therefore, N125 and S123 are critical residues for the inhibition of FBPase by disulfiram derivatives.

LC-MS and Mutation Experiments

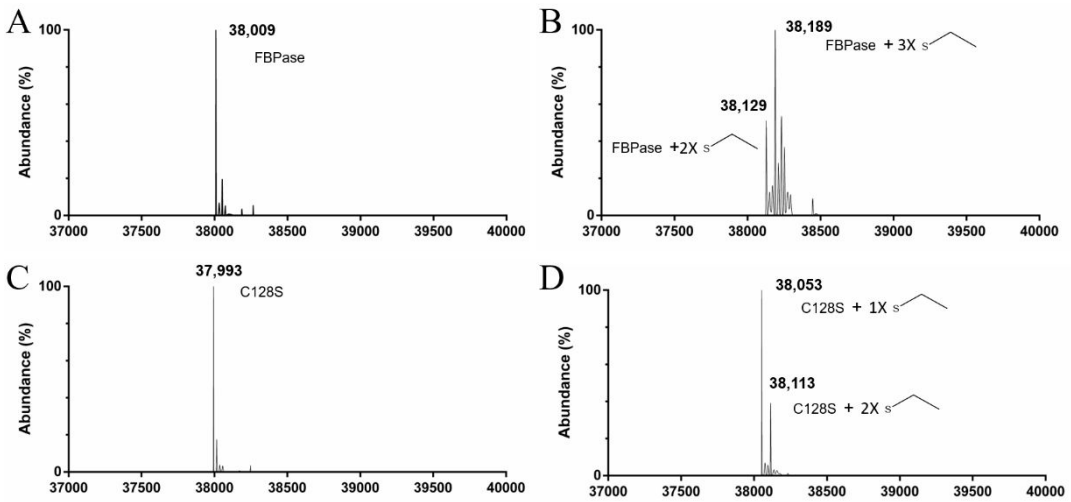

Fig. 4. Full scan electrospray mass spectrum of the parent ion region of **214** covalent binding of WT (wild type) FBPase and C128S. (A) The molecular weight of WT FBPase; (B) Mass weight of FBPase + *n***214b** (*n* = 2, 3); (C) Mass weight of C128S mutation; (D) Mass weight of C128S + *n***214b** (*n* = 1, 2).

Liquid chromatography-mass spectrometry (LC-MS) was performed to verify whether these compounds covalently bind C128 in FBPase. As illustrated in Fig. 4A, the molecular weight of FBPase is 38,009 Da. Correspondingly, the peaks at 38,129 Da

(FBPase+2*__214b__) and 38,189 Da (FBPase+3*__214b__) in Fig. 4B match the molecular weight of FBPase covalently bound to two and three **214b** fragments of **214**, which indicates that **214b** could covalently bind to multiple cysteines in FBPase. The peak of 37,993 Da in Fig. 4C corresponds to the molecular weight of the C128S mutation (when the C128 residue in FBPase was mutated to serine). Notably, Fig. 4D shows peaks of 38,053 Da (C128S+**214b**) and 38,113 Da (C128S+2*__214b__), which indicate that **214b** could covalently bind with cysteines in FBPase other than C128. The peaks in the LC-MS spectrum of wild type FBPase (Fig. 4B) show that one equivalent of the **214b** fragment was lost in the peaks of C128S (Fig. 4D), which implied that **214b** was most likely covalently bound to C128. In fact, the crystallographic data mentioned above have already lent a solid credit for this finding. In addition, the possible reaction pathway between FBPase and 214 was illustrated in Fig. S3. In addition, the possible reaction mechanism between FBPase and compound **212** was also predicted by using XO methods at ωB97X-D/6-31G*//ωB97X-D/6-311-G** theoretical level, as shown in Fig. S4.

To identify the central and important role of cysteine in covalent inhibitory regulation, when FBPase was covalently modified by disulfiram and its derivatives, the IC_{50} values of these three compounds against cysteine mutants were measured systematically.

Table 2. The IC_{50} of Disulfiram/**212**/**214** against cysteine mutation and WT FBPase

	WT	C38S	C92S	C116S	C128S	C179S	C183S	C281S
k_{cat} (s^{-1})	2.5±0.1	0.80±0.06	0.99±0.06	0.99±0.12	1.7±0.1	1.4±0.1	2.3±0.1	2.2±0.1
Disulfiram IC_{50} (μM)	1.5±0.1	0.60±0.03	1.2±0.1	1.3±0.06	> 1000[a]	1.9±0.2	1.5±0.2	1.1± 0.1
Disulfiram (IC^M_{50} / IC^W_{50})	1	0.4	0.8	0.9	> 667	1.3	1	0.7
212 IC_{50} (μM)	0.54±0.06	2.1±0.7	0.64±0.12	0.85±0.08	> 1000[a]	0.67±0.06	1.1± 0.1	1.3± 0.1
212 (IC^M_{50} / IC^W_{50})	1	3.8	1.2	1.6	> 1800	1.2	2.1	2.5
214 IC_{50} (μM)	1.6±0.2	6.6±1.0	0.98±0.26	1.9±0.3	> 1000[a]	1.8±0.2	1.2± 0.3	1.5± 0.2
214 (IC^M_{50} / IC^W_{50})	1	4.1	0.6	1.2	> 625	1.1	0.75	0.93

[a]1000 μM inhibition rate is less than 50%

As shown in Table 2, the IC_{50} values of **212**, **214** and disulfiram against the C38S, C92S, C116S, C179S, C183S and C281S mutants were almost the same as their IC_{50} values against the wild type (WT) protein, and only the C128S mutation resulted in a significant increase (>600-fold) in the IC_{50} values compared to that of the WT protein. The above mutant assays and crystallographic data show that C128 plays a unique and crucial role in the covalent allosteric inhibition of FBPase when disulfiram, **212**, and **214** covalently bind with FBPase.

In addition, a series of Ala mutation assays of residues S123, S124 and N125 in helix H4 were carried out, and the corresponding IC_{50} values of disulfiram**, 212** and **214** against these mutants were determined as well. The enzymatic activities of S123A, S124A and N125A were determined as described in our previous report[25]. Compared with the WT (k_{cat}=2.5 s^{-1}), S124A (k_{cat}=3.1 s^{-1}) and N125A (k_{cat}=0.93 s^{-1}) retained comparable catalytic activities, while S123A (k_{cat}=0.04 s^{-1}) lost almost all of its catalytic activity[25]. Thus, these results demonstrated that among the above three

residues, only S123 was crucial for the catalytic activity of the enzyme, which was consistent with the crystallographic structure of FBP-bound (PDB:5ZWK), showing a direct interaction between S123 and the substrate. As listed in Table S1, the IC_{50} values of disulfiram, **212** and **214** against the S124A mutant of FBPase showed almost no changes compared to those of WT FBPase, however, the N125A mutation led to 320-, 900- and 313-fold increases in the IC_{50} values of disulfiram, **212** and **214**, respectively, indicating that N125 but not S124 played an important role in the covalent allosteric inhibitory regulation of helix H4 when C128 was covalently bound with these disulfiram derivatives. Notably, the results of this mutation assay are consistent with the abovementioned MD results and helpful for further understanding the inhibitory regulation mechanism of new covalent allosteric binding sites through the dissociation of helix H4 in FBPase.

Glucose Reduction in ICR and *db*/*db* Mice

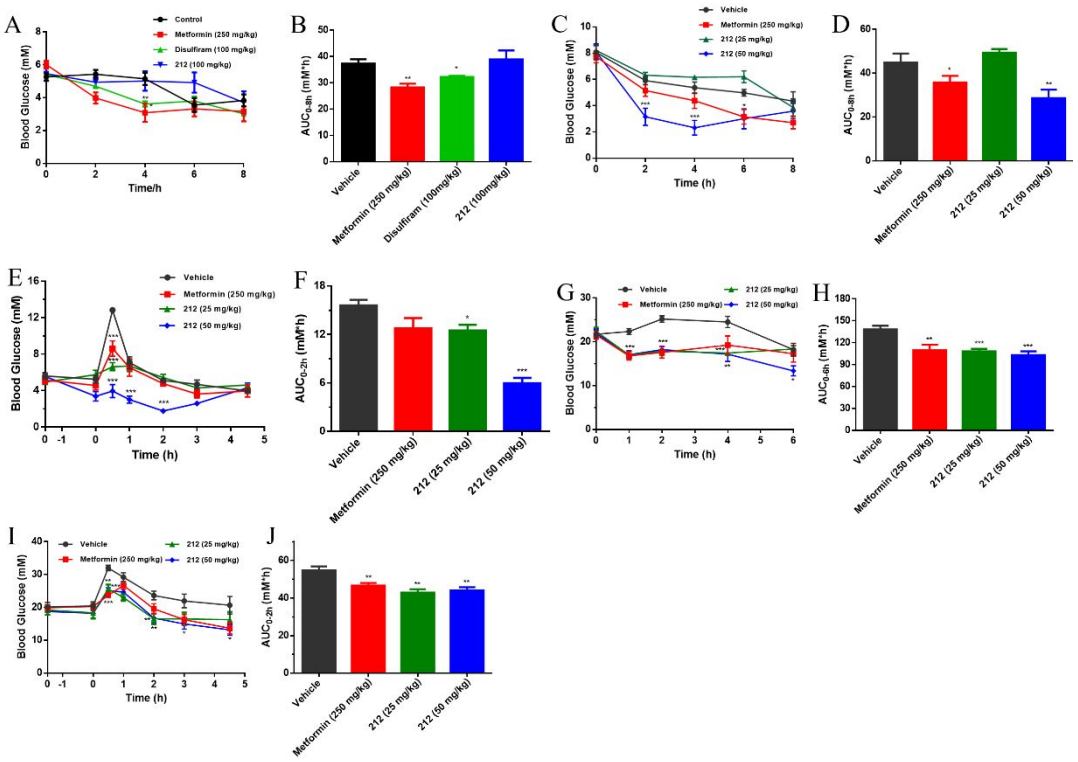

Fig. 5. Effect of a single administration of disulfiram or compound **212** on blood glucose in 7-9 weeks old ICR mice or *db/db* mice (n = 5-6 in each group). (A) and (B) Blood glucose changes and AUC of blood glucose between 0 and 8 h in 12 h-fasted ICR mice after oral administration of disulfiram and compound **212**. (C) and (D) Blood glucose changes and AUC of blood glucose between 0 and 8 h in 12 h-fasted ICR mice after intraperitoneal administration of compound **212**. (E) and (F) Blood glucose responses to an oral glucose challenge (2 g/kg) and AUC of blood glucose between 0 and 2 h in 12 h-fasted ICR mice. Compound **212** was intraperitoneally administered 1.5 h prior to oral glucose challenge. (G) and (H) Blood glucose changes and AUC of blood glucose between 0 and 6 h in freely feeding *db/db* mice after intraperitoneal administration of compound **212**. (I) and (J) Blood glucose responses to an oral glucose challenge (2 g/kg) and AUC of blood glucose between 0 and 2 h in 12 h-fasted *db/db* mice. Compound **212** was administered 1.5 h prior to oral glucose challenge. Data are presented as the mean ± SEM. (*) $P < 0.05$, (**) $P < 0.01$, (***) $P < 0.001$ vs vehicle. Student's *t* test.

Considering the better FBPase inhibitory activities of disulfiram and **212**, it is imperative to further evaluate the hypoglycemic efficacies of these two compounds in ICR and *db/db* mice. As shown in Fig. 5A, in an oral administration model, disulfiram at doses of 100 mg/kg significantly reduced blood glucose at 4 h ($p < 0.01$ vs vehicle), and the area under the curve $(AUC)_{0\text{-}8h}$ of the 100 mg/kg disulfiram treated group was reduced by 12.8% compared to that of the vehicle group (Fig. 5B). However, compound **212** at oral doses of 100 mg/kg failed to display hypoglycemic effect, most likely due to its poor oral bioavailability. Interestingly, we found that compound **212** at an intraperitoneal dose of 50 mg/kg could remarkably reduce blood glucose in mice during 2 h to 6 h compared to that of the vehicle group at 50 mg/kg (Fig. 5C). $AUC_{0\text{-}8h}$ analysis suggested that the 50 mg/kg **212** treated group exhibited a 36.3% reduction in blood glucose (Fig. 5D). Unfortunately, disulfiram cannot be administered intraperitoneally

due to its poor water solubility. Therefore, **212** was selected for further pharmacodynamics studies. To better evaluate glucose tolerance in response to treatment with **212**, an oral glucose tolerance test (OGTT) was carried out in ICR mice. Glucose challenge (2 g/kg) dramatically increased the blood glucose levels in the vehicle group, whereas the **212** administered groups exhibited much smaller increases in blood glucose, especially at 30 min after glucose administration (Fig. 5E). The $AUC_{0\text{-}2h}$ analysis suggested that 50 mg/kg **212** observably increased glucose tolerance by reducing the $AUC_{0\text{-}2h}$ by 61.7% relative to that of the vehicle group, and the pharmaceutical effect was superior to that of 25 mg/kg **212** ($\Delta AUC_{0–2h}$ = 19.8%) (Fig. 5F). These results clearly demonstrated that disulfiram and **212** have hypoglycemic effects in ICR mice.

As an important pathway for glucose homeostasis, GNG can convert lactate and other carbon substrates into glucose (Fig. S5A). Therefore, the inhibition of FBPase likely blocks the GNG pathway and leads to decreased glucose and lactate concentrations. To preliminarily determine whether compound **212** could inhibit FBPase *in vivo*, we measured several parameters in ICR mice, including the concentrations of blood glucose, blood lactate and the FBPase activity. As illustrated in Fig. S5B, compound **212** at a dose of 50 mg/kg had hypoglycemic effects ($P < 0.05$ vs vehicle) 2 h after i.p. administration. At the same time, the blood lactate concentration of the **212**-treated group (4.1 mM) was elevated relative to that of the vehicle group (2.0 mM) (Fig. S5C) but lactic acidosis was not observed (>5 mM [33]). Moreover, **212** significantly inhibited the activity of FBPase at 50 mg/kg (Fig. S5D).

These results further indicate that compound **212** could block GNG by inhibiting FBPase.

In light of the favorable hypoglycemic effect of **212** in ICR mice, the ability of **212** to lower glucose was further evaluated in diabetic *db/db* mice. Low doses (25 mg/kg and 50 mg/kg) of **212** had hypoglycemic effects at 1-4 h compared to the vehicle (Fig. 5G), and remarkably reduced blood glucose $AUC_{0\text{-}6h}$ by 21.7% and 25.5%, respectively (Fig. 5H). An OGTT was also performed to evaluate the glucose tolerance ability of **212**. $AUC_{0\text{-}2h}$ analysis suggested that compound **212** at a dose of 25 mg/kg observably increased glucose tolerance by reducing the $AUC_{0\text{-}2h}$ by 21.8% relative to the vehicle, which was similar to the effect of **212** at 50 mg/kg (ΔAUC_{0-2h} = 19.7%) (Fig. 5I and 5J). These experiments suggested that **212** could also improve glucose homeostasis in diabetic *db/db* mice.

CONCLUSIONS

In this study, a novel covalent allosteric binding site, which is distinct from the original C128 site in APO FBPase and not exploited by previous works, was discovered based on the cocrystal structure of FBPase-**214b**. Disulfiram, a well-known anti-alcoholism drug, and its derivatives (**212** and **214)** were found to potently inhibit FBPase by covalently binding to this new C128 site. Crystallographic and MD studies revealed that the addition of **214b** to C128 would repel N125 away from C128, and disrupt the S124--C128 hydrogen-bond and helix H4 (123-128). The dissociation of helix H4 allows S123 to more easily move away from FBP and form a new hydrogen-bond with K71, which in turn results in the extension of helix H3 (69-72). The

hydrogen-bond of S123--FBP is essential for the catalytic activity of FBPase, and the addition of **214b** to C128 could disrupt the S123--FBP hydrogen bond and thereby inhibiting FBPase. To the best of our knowledge, this is the first report that disulfiram or its derivatives act as covalent allosteric modulators of FBPase and exhibit hypoglycemic effects. In particular, disulfiram and **212** moderately reduced blood glucose in an ICR mouse model and a *db/db* mouse model. Our current findings identify a new covalent allosteric binding site of FBPase, and establish a structural foundation for the discovery of new covalent allosteric drugs that inhibit FBPase.

EXPERIMENTAL SECTION

Chemistry. The synthetic starting materials, reagents, and solvents were obtained from a commercial supplier, such as Energy Chemical, J&K, and TCI at the highest commercial quality and were used without further purification. The reaction progress was monitored using analytical thin layer chromatography (TLC), HSGF 254 (150-200 μm thickness; Yantai Huiyou Co., China), UV light (254 nm) and I2 were used to visualize the components. ^{1}H NMR and ^{13}C NMR spectra were recorded on a Bruker AMX 400 and AMX 600 spectrometer in DMSO-d6, or $CDCl_3$ with TMS as an internal standard. Chemical shifts are reported in parts per million (ppm, δ) downfield from tetramethylsilane. Proton coupling patterns are described as singlet (s), doublet (d), triplet (t), quartet (q), and multiplet (m). High-resolution mass spectrometry (HRMS) data were obtained by electron ionization (EI) using a Waters GCT Premier. All final compounds were purified to > 95% purity, as determined by high-performance liquid chromatography (HPLC) on an Agilent 1100 instrument with a quaternary pump and a

diode array detector (DAD), MeOH:H_2O=95:5 (v:v) as the eluent, and a flow rate of 0.5 mL/min.

*2-((4-Chlorophenyl)disulfanyl)thiazole (**212**)*. To a stirred solution of 4-chlorobenzenethiol (1.4 g, 10 mmol) in 20 mL of anhydrous dichloromethane was added dropwise sulfuryl chloride (810 μL, 10 mmol) at 0 °C. The reaction mixture was stirred for 1 h at the same temperature and then concentrated under reduced pressure to afford 4-chlorophenyl hypochlorothioite as a brownish yellow liquid, which was used in the next step without purification. A solution of freshly prepared 4-chlorophenyl hypochlorothioite (5 mmol) in 10 mL of anhydrous ethyl ether was added dropwise to a solution of thiazole-2-thiol (5 mmol) in 10 mL of anhydrous ethyl ether at room temperature. The reaction mixture was stirred for 12 h, and removal of the solvents produced a liquid that was purified using column chromatography, to afford compound **212**. Yellow liquid. 75% yield. ^{1}H NMR (400 MHz, $CDCl_3$) δ 7.73 (d, J = 3.3 Hz, 1H), 7.57–7.50 (m, 2H), 7.34 –7.29 (m, 3H). ^{13}C NMR (151 MHz, DMSO) δ 144.93, 130.91, 130.03, 129.92, 129.62, 124.03. HRMS (EI): m/z calcd $C_9H_6ClNS_3$ (M^+) 258.9351, found 258.9352. HPLC purity: 99.2%.

*2-(Ethyldisulfanyl)benzo[d]thiazole (**214**)*. 2-Mercaptobenzothiazole (1.0 mmol) and ethanethiol (1.5 mmol) were dissolved in 5 mL of DCM at 0 °C. DDQ (1.0 mmol) was then slowly added in portions to the solution, and the reaction mixture was stirred for 0.5−1 h on an ice bath. Upon completion of the reaction, the solvents were evaporated under vacuum, and the crude compound was purified via column chromatography to give compound **214**. Colorless oil. 85% yield. ^{1}H NMR (400 MHz,

$CDCl_3$) δ 7.87 (d, *J* = 8.1 Hz, 1H), 7.80 (dd, *J* = 8.0, 0.5 Hz, 1H), 7.47–7.40 (m, 1H), 7.36–7.30 (m, 1H), 2.98 (q, *J* = 7.3 Hz, 2H), 1.42 (t, *J* = 7.3 Hz, 3H). ^{13}C NMR (150 MHz, DMSO-d_6) δ 172.79, 155.13, 135.72, 126.99, 125.25, 122.46, 122.18, 33.26, 14.62. HRMS (EI) m/z calcd $C_9H_9NS_3$ $[M]^+$ 226.9897, found 226.9894. HPLC purity: 99.9%.

Drugs and Chemicals. Mercaptopurine, furazolidone, disulfiram, carmofur, lipoic acid, afatinib, phosphonomycin, eflornithine, warfarin and phenoxybenzamine were obtained from Sigma-Aldrich.

Enzyme Activity Assays and Mutagenesis. Full-length WT human liver FBPase (GenBank: D26055.1) was expressed in *E.coli* BL21 (DE3) and purified with a HisTrap_FF_5 mL [Global] column following the standard ÄKTA™ pure system, and this process was performed as described in our previous work.[34] Enzymatic reactions were performed with purified enzyme (11.2 μg/mL), and FBP (0.4 mM/L) in 30 μL of buffer (50 mM/L Tris, 0.8 mM/L Mg^{2+}). After reacting for 5 min at 37 ℃, 15 μL of 1 M perchloric acid was used to stop the reaction, and then malachite green (0.35% polyvinyl alcohol and 0.0035% malachite green) was added to quantify the inorganic phosphate. The A620 was measured after these additions.[25] The kinetic constants values or half maximal inhibitory concentration (IC_{50}) were identified using logistic equations (nonlinear analysis) or Hill kinetic equations in the Origin 7.5 program package.

Mutations were performed by introducing specific base changes into a double-stranded DNA plasmid. The mutant constructs were generated using the two-step PCR method. DNA encoding WT human liver FBPase cloned into pET-21b was used as a

template for mutagenesis. The parental methylated and hemimethylated DNA were digested by Nde I and Xhol1 restriction enzymes. Then, the mutant constructs were ligated into a previous plasmid. The plasmids of the recombinant mutant were transformed into DH5α competent cells. All of the mutations were confirmed by DNA sequencing. The verified plasmids with mutations were transformed into strain *E.coli* BL21 (DE3) cells. The mutant FBPase proteins were purified in the same manner as WT FBPase.

Crystallization, Data Collection and Structure Determination. APO FBPase crystals were obtained after 5-7 days at 18 ℃ by the hanging drop vapor diffusion method against 500 μL of well solution using 24-well crystallization plates. The crystallization drops contained 1 μL of protein solution (10 mg/mL FBPase, 0.1 M NaCl, 1 mM AMP and 10 mM Mg^{2+}) mixed with 1 μL of reservoir solution containing 0.05 M Tris (pH 6.8) and 10% (v/v) polyethylene glycol 8000. **214** was soaked into the drop of APO FBPase crystals by adding 0.2 μL of the compound (5 mM) in the same reservoir solution for 10 h.

Crystals were cryoprotected with 20% (v/v) glycerol and flash-cooled in liquid nitrogen. The data were acquired at the Shanghai Synchrotron Radiation Facility on beamline BL19U. The data were processed with XDS packages.[35] Furthermore, the structure was solved by molecular replacement using the CCP4[36] program and a previous human FBPase structure (PDB ID: 5ZWK) was used as the search model. Model analysis, building and refinement were performed with the Coot[37] and Phenix[38] programs.

Animals. Male ICR mice (6-7 weeks) and male BKS. Cg-+Leprdb/+Leprdb/JclSlac mice (6-8 weeks) were purchased from Shanghai JSJ Lab Animal, Ltd. and Shanghai SLAC Laboratory Animal Co., respectively. The animals were housed under specific pathogen-free conditions with a 12-h light-dark cycle, at a temperature of 25 °C, humidity of 55%, and free access to water and food. The animal study was approved by the Animal Care and Use Committee of Central China Normal University

Glucose Reduction in ICR Mice. ICR mice that had been fasted for 12 h (n = 6 in each group) were administered vehicle (10% Ricinus oil in water), **212** (100 mg/kg, p.o.), disulfiram (100 mg/kg p.o.) or compound **212** (25 mg/kg and 50 mg/kg, i.p.). Food was withheld throughout the study. Blood samples were obtained from the tail vein at 0, 2, 4, 6 and 8 h and were analyzed using a glucometer (Sanicare).

Glucose Reduction in *db/db* Mice. Freely fed *db/db* mice (n = 6 in each group) were intraperitoneally administered compound **212** (25 mg/kg and 50 mg/kg), metformin (250 mg/kg), or vehicle (10% Ricinus oil in water). Food was withheld after the administration of the test compounds. Blood samples were obtained from the tail vein at 0, 2, 4 and 6 h and were analyzed using a glucometer (Sanicare).

OGTT in ICR Mice and *db/db* Mice. ICR mice or *db/db* mice that had been fasted for 12 h (n = 6 in each group) were intraperitoneally administered compound **212** (25 mg/kg and 50 mg/kg), metformin (250 mg/kg), or vehicle (10% Ricinus oil in water) 1.5 h before glucose challenge. Glucose (2 g/kg) was orally administered at 0 h, and blood samples were drawn from the tail vein at 0, 0.5, 1, 2, 3, and 4.5 h after glucose

administration. Plasma glucose was measured using a glucometer (Sanicare). Food was withheld throughout the study.

Inhibition of FBPase *ex vivo*. ICR mice received the test compound *via* i.p. administration and were euthanized by decapitation after 2 h. The liver was removed, weighed, and homogenized in double distilled water. Blood samples were obtained from the tail vein at 0 h and 2 h. The activities of liver FBPase were tested as previously described.[1] Blood glucose was measured using a glucometer, and blood lactate was measured using a Lactic Acid LD Assay Kit (Nanjing Jiancheng Bioengineering Institute).

Mass Spectrometry. WT FBPase (50 μM) or C128S FBPase (50 μM) was incubated with 500 μM disulfiram and **212** for 2 h. Then, the samples were analyzed using an Agilent 6550 quadrupole-time-of-flight (QTOF) mass spectrometer (Santa Clara, CA) coupled with an Agilent 1260 high-performance liquid chromatograph (HPLC; Santa Clara, CA).

The samples were separated on a Phenomenex Jupiter C4 300 Å LC column (2×150 mm, 5 μm) over 15 min using a gradient from 5% to 100% acetonitrile containing 0.1% formic acid at a flow rate of 0.5 mL/min. Data were acquired in positive-ion mode with Dual Agilent Jet Stream electrospray voltage using a capillary temperature of 250 °C, a fragmentor voltage of 175 V, a capillary voltage of 3000 V, and a m/z 600−3200 mass window. Mass deconvolution was then performed using Agilent Mass Hunter Qualitative Analysis B.06.00 software.

Molecular Dynamic Simulations. The crystal structures of the apo state (1FTA), FBP-

bound state (5ZWK) and FBP/**214b**-bound state obtained in this study were used as templates to set up the system for MD simulations. The CHARMM force field[39] and CGENFF force field[40] were used for the protein and the ligands (including FBP and **214b**), respectively. The whole system was surrounded by TIP3P water molecules[41] in a truncated octahedral box 10 Å from any solute atoms. The system was neutralized with K^+ counterions. MD simulations of 100 ns were performed at 300 K. LINCS[42] was used to constrain bonds involving hydrogen atoms, and the time step was 2.0 fs. The nonbonded cutoff was set to 10 Å. The long-range electrostatics were calculated by the particle mesh Ewald (PME) algorithm.[43] Parallel simulations were performed simultaneously using GROMACS 5.1.4.[44] To characterize the changes in the secondary structures at helix E, *i.e.*, residues 120-129, the collective variable ALPHARMSD[32] was used to probe the number of six-residue segments in the α-helical configuration.

ASSOCIATED CONTENT

Supporting information.

The Supporting Information is available free of charge at (http://pubs.acs.org). Molecular formula strings (CSV); molecular dynamic results (PDB); ^{1}H NMR, ^{13}C NMR, and high-resolution mass spectra (HRMS) data; HPLC spectra data for **212**/**214**; WT and mutant enzyme data and proposed reaction mechanism calculation for **212** (PDF).

Accession code.

The atomic coordinates and structure factors have been deposited into the RCSB Protein Data Bank with accession numbers 6LS5. Authors will release the atomic

coordinates and experimental data upon article publication.

AUTHOR INFORMATION

Corresponding Authors

Jian Wan: *Key Laboratory of Pesticide & Chemical Biology (CCNU), Ministry of Education, College of Chemistry, Central China Normal University, Wuhan 430079, China*; Email: jianwan@mail.ccnu.edu.cn; Phone: +86-27-67862022. Fax: +86-27-67862022

Yanliang Ren: *Key Laboratory of Pesticide & Chemical Biology (CCNU), Ministry of Education, College of Chemistry, Central China Normal University, Wuhan 430079, China*; E-mail: renyl@mail.ccnu.edu.cn; Phone: +86-27-67862022. Fax: +86-27-67862022

Jian Li: *Shanghai Key Laboratory of New Drug Design, School of Pharmacy, East China University of Science and Technology, Shanghai 200237, China;* E-mail: jianli@ecust.edu.cn; Phone: +86-21-64252584. Fax: +86-21-64252584.

Authors

Yunyuan Huang: *Key Laboratory of Pesticide & Chemical Biology (CCNU), Ministry of Education, College of Chemistry, Central China Normal University, Wuhan 430079, China*

Yixiang Xu: *Shanghai Key Laboratory of New Drug Design, School of Pharmacy, East China University of Science and Technology, Shanghai 200237, China*

Rongrong Song: *Key Laboratory of Pesticide & Chemical Biology (CCNU), Ministry of Education, College of Chemistry, Central China Normal University, Wuhan 430079,*

China

Shuaishuai Ni: *Cancer Institute, Longhua Hospital, Shanghai University of Traditional Chinese Medicine, Shanghai, 200032, China*

Jiaqi Liu: *Key Laboratory of Pesticide & Chemical Biology (CCNU), Ministry of Education, College of Chemistry, Central China Normal University, Wuhan 430079, China*

Yanhong Xu: *Key Laboratory of Pesticide & Chemical Biology (CCNU), Ministry of Education, College of Chemistry, Central China Normal University, Wuhan 430079, China*

Li Rao: *Key Laboratory of Pesticide & Chemical Biology (CCNU), Ministry of Education, College of Chemistry, Central China Normal University, Wuhan 430079, China*

Yingjie Wang: *Shenzhen Bay Laboratory, Shenzhen 518055, Guangdong, China*

Lin Wei: *Key Laboratory of Pesticide & Chemical Biology (CCNU), Ministry of Education, College of Chemistry, Central China Normal University, Wuhan 430079, China*

Lingling Feng: *Key Laboratory of Pesticide & Chemical Biology (CCNU), Ministry of Education, College of Chemistry, Central China Normal University, Wuhan 430079, China*

Chen Su: *National Facility for Protein Science in Shanghai, Zhangjiang Lab, Shanghai, 201210, China*

Chao Peng: *National Facility for Protein Science in Shanghai, Zhangjiang Lab,*

Shanghai, 201210, China

Author Contributions

All authors contributed to the writing of the manuscript and have approved the final version of the manuscript. #These authors contributed equally. (Match statement to author names with a symbol)

Notes

The authors declare no competing financial interest.

ACKNOWLEDGMENTS

This work was supported by the Natural Science Foundation of China (Nos. 21877046, 21873035, 21572077 and 21472061), the Program for the PCSIRT (No. IRT0953), and the self-determined research funds of CCNU from the colleges' basic research and operation of MOE (Nos. CCNU19TS011, CCNU18TS010, 2018YBZZ019 and CCNU16A02041), the support from the Program of Introducing Talents of Discipline to Universities of China (111 Program, B17019) is also appreciated. We thank the staff of the BL19U1 beamline of the NCPSS at the Shanghai Synchrotron Radiation Facility for assistance during data collection.

Abbreviations

FBPase: fructose-1,6-bisphosphatase; FBP: fructose-1,6-biphosphate; F6P: fructose-6-biphosphate; IC_{50}: half maximal inhibitory concentration; T2D: Type 2 diabetes; AMP: adenosine monophosphate; ICR: Institute of Cancer Research; OGTT: oral glucose

tolerance test; LC-MS: liquid chromatography−mass spectrometry; GNG: gluconeogenesis;

REFERENCES

(1) Hunter, R. W.; Hughey, C. C.; Lantier, L.; Sundelin, E. I.; Peggie, M.; Zeqiraj, E.; Sicheri, F.; Jessen, N.; Wasserman, D. H.; Sakamoto, K. Metformin reduces liver glucose production by inhibition of fructose-1-6-bisphosphatase. *Nat. Med.* **2018,** 24, 1395-1406.

(2) Li, B.; Qiu, B.; Lee, D. S.; Walton, Z. E.; Ochocki, J. D.; Mathew, L. K.; Mancuso, A.; Gade, T. P.; Keith, B.; Nissim, I.; Simon, M. C. Fructose-1,6-bisphosphatase opposes renal carcinoma progression. *Nature* **2014,** 513, 251-255.

(3) Huangyang, P.; Li, F.; Lee, P.; Nissim, I.; Weljie, A. M.; Mancuso, A.; Li, B.; Keith, B.; Yoon, S. S.; Simon, M. C. Fructose-1,6-Bisphosphatase 2 Inhibits Sarcoma Progression by Restraining Mitochondrial Biogenesis. *Cell Metab.* **2020,** 31, 174-188.

(4) Dong, C.; Yuan, T.; Wu, Y.; Wang, Y.; Fan, T. W.; Miriyala, S.; Lin, Y.; Yao, J.; Shi, J.; Kang, T.; Lorkiewicz, P.; St Clair, D.; Hung, M. C.; Evers, B. M.; Zhou, B. P. Loss of FBP1 by Snail-mediated repression provides metabolic advantages in basal-like breast cancer. *Cancer Cell* **2013,** 23, 316-331.

(5) Cong, J.; Wang, X.; Zheng, X.; Wang, D.; Fu, B.; Sun, R.; Tian, Z.; Wei, H. Dysfunction of Natural Killer Cells by FBP1-Induced Inhibition of Glycolysis during Lung Cancer Progression. *Cell Metab.* **2018,** 28, 243-255.

(6) Guo, B.; Huang, X.; Lee, M. R.; Lee, S. A.; Broxmeyer, H. E. Antagonism of PPAR-gamma signaling expands human hematopoietic stem and progenitor cells by enhancing glycolysis. *Nat. Med.* **2018,** 24, 360-367.

(7) Rines, A. K.; Sharabi, K.; Tavares, C. D. J.; Puigserver, P. Targeting hepatic glucose metabolism in

the treatment of type 2 diabetes. *Nat. Rev. Drug Discov.* **2016,** 15, 786-804.

(8) Kaur, R.; Dahiya, L.; Kumar, M. Fructose-1,6-bisphosphatase inhibitors: A new valid approach for management of type 2 diabetes mellitus. *Eur. J. Med. Chem.* **2017,** 141, 473-505.

(9) Bie, J.; Liu, S.; Li, Z.; Mu, Y.; Xu, B.; Shen, Z. Discovery of novel indole derivatives as allosteric inhibitors of fructose-1,6-bisphosphatase. *Eur. J. Med. Chem.* **2015,** 90, 394-405.

(10) van Poelje, P. D.; Potter, S. C.; Chandramouli, V. C.; Landau, B. R.; Dang, Q.; Erion, M. D. Inhibition of fructose 1,6-bisphosphatase reduces excessive endogenous glucose production and attenuates hyperglycemia in Zucker diabetic fatty rats. *Diabetes* **2006,** 55, 1747-1754.

(11) Dang, Q.; Van Poelje, P. D.; Erion, M. D. The Discovery and Development of MB07803, a Second-Generation Fructose-1,6-bisphosphatase Inhibitor with Improved Pharmacokinetic Properties, as a Potential Treatment of Type 2 Diabetes. *in: R.M. Jones (Ed.), New Therapeutic Strategies for Type 2 Diabetes: Small Molecule Approaches, Royal Society of Chemistry, London* **2012**, 306-323.

(12) Dang, Q.; Kasibhatla, S. R.; Reddy, K. R.; Jiang, T.; Reddy, M. R.; Potter, S. C.; Fujitaki, J. M.; van Poelje, P. D.; Huang, J.; Lipscomb, W. N.; Erion, M. D. Discovery of potent and specific fructose-1,6-bisphosphatase inhibitors and a series of orally-bioavailable phosphoramidase-sensitive prodrugs for the treatment of type 2 diabetes. *J. Am. Chem. Soc.* **2007,** 129, 15491-15502.

(13) Erion, M. D.; Dang, Q.; Reddy, M. R.; Kasibhatla, S. R.; Huang, J.; Lipscomb, W. N.; van Poelje, P. D. Structure-guided design of AMP mimics that inhibit fructose-1,6-bisphosphatase with high affinity and specificity. *J. Am. Chem. Soc.* **2007,** 129, 15480-15490.

(14) Nussinov, R.; Tsai, C. J. Allostery in disease and in drug discovery. *Cell* **2013,** 153, 293-305.

(15) Lu, S.; Shen, Q.; Zhang, J. Allosteric Methods and Their Applications: Facilitating the Discovery of Allosteric Drugs and the Investigation of Allosteric Mechanisms. *Acc. Chem. Res.* **2019,** 52, 492-500.

(16) Lonsdale, R.; Ward, R. A. Structure-based design of targeted covalent inhibitors. *Chem. Soc. Rev.* **2018,** 47, 3816-3830.

(17) Singh, J.; Petter, R. C.; Baillie, T. A.; Whitty, A. The resurgence of covalent drugs. *Nat. Rev. Drug Discov.* **2011,** 10, 307-317.

(18) Lu, S.; Zhang, J. Designed covalent allosteric modulators: an emerging paradigm in drug discovery. *Drug Discov. Today* **2017,** 22, 447-453.

(19) Nussinov, R.; Tsai, C. J. The design of covalent allosteric drugs. *Annu. Rev. Pharmacol. Toxicol.* **2015,** 55, 249-267.

(20) Uhlenbrock, N.; Smith, S.; Weisner, J.; Landel, I.; Lindemann, M.; Le, T. A.; Hardick, J.; Gontla, R.; Scheinpflug, R.; Czodrowski, P.; Janning, P.; Depta, L.; Quambusch, L.; Müller, M. P.; Engels, B.; Rauh, D. Structural and chemical insights into the covalent-allosteric inhibition of the protein kinase Akt. *Chem. Sci.* **2019,** 10, 3573-3585.

(21) Jonathan M. Ostrem; Ulf Peters; Martin L. Sos; James A. Wells; Shokat, K. M. K-Ras(G12C) inhibitors allosterically control GTP affinity and effector interactions. *Nature* **2013,** 503, 548-551.

(22) Janes, M. R.; Zhang, J.; Li, L. S.; Hansen, R.; Peters, U.; Guo, X.; Chen, Y.; Babbar, A.; Firdaus, S. J.; Darjania, L.; Feng, J.; Chen, J. H.; Li, S.; Li, S.; Long, Y. O.; Thach, C.; Liu, Y.; Zarieh, A.; Ely, T.; Kucharski, J. M.; Kessler, L. V.; Wu, T.; Yu, K.; Wang, Y.; Yao, Y.; Deng, X.; Zarrinkar, P. P.; Brehmer, D.; Dhanak, D.; Lorenzi, M. V.; Hu-Lowe, D.; Patricelli, M. P.; Ren, P.; Liu, Y. Targeting KRAS Mutant Cancers with a Covalent G12C-Specific Inhibitor. *Cell* **2018,** 172, 578-589.

(23) Canon, J.; Rex, K.; Saiki, A. Y.; Mohr, C.; Cooke, K.; Bagal, D.; Gaida, K.; Holt, T.; Knutson, C. G.; Koppada, N.; Lanman, B. A.; Werner, J.; Rapaport, A. S.; San Miguel, T.; Ortiz, R.; Osgood, T.; Sun, J. R.; Zhu, X.; McCarter, J. D.; Volak, L. P.; Houk, B. E.; Fakih, M. G.; O'Neil, B. H.; Price, T. J.;

Falchook, G. S.; Desai, J.; Kuo, J.; Govindan, R.; Hong, D. S.; Ouyang, W.; Henary, H.; Arvedson, T.; Cee, V. J.; Lipford, J. R. The clinical KRAS(G12C) inhibitor AMG 510 drives anti-tumour immunity. *Nature* **2019,** 575, 217-223.

(24) Lanman, B. A.; Allen, J. R.; Allen, J. G.; Amegadzie, A. K.; Ashton, K. S.; Booker, S. K.; Chen, J. J.; Chen, N.; Frohn, M. J.; Goodman, G.; Kopecky, D. J.; Liu, L.; Lopez, P.; Low, J. D.; Ma, V.; Minatti, A. E.; Nguyen, T. T.; Nishimura, N.; Pickrell, A. J.; Reed, A. B.; Shin, Y.; Siegmund, A. C.; Tamayo, N. A.; Tegley, C. M.; Walton, M. C.; Wang, H. L.; Wurz, R. P.; Xue, M.; Yang, K. C.; Achanta, P.; Bartberger, M. D.; Canon, J.; Hollis, L. S.; McCarter, J. D.; Mohr, C.; Rex, K.; Saiki, A. Y.; San Miguel, T.; Volak, L. P.; Wang, K. H.; Whittington, D. A.; Zech, S. G.; Lipford, J. R.; Cee, V. J. Discovery of a Covalent Inhibitor of KRAS(G12C) (AMG 510) for the Treatment of Solid Tumors. *J. Med. Chem.* **2020,** 63, 52-65.

(25) Huang, Y.; Wei, L.; Han, X.; Chen, H.; Ren, Y.; Xu, Y.; Song, R.; Rao, L.; Su, C.; Peng, C.; Feng, L.; Wan, J. Discovery of novel allosteric site and covalent inhibitors of FBPase with potent hypoglycemic effects. *Eur. J. Med. Chem.* **2019,** 184, 111749.

(26) Veverka, K. A.; Johnson, K. L.; Mays, D. C.; Lipsky, J. J.; Naylor, S. Inhibition of aldehyde dehydrogenase by disulfiram and its metabolite methyl diethylthiocarbamoyl-sulfoxide. *Biochem. Pharmacol.* **1997,** 53, 511-518.

(27) Skrott, Z.; Mistrik, M.; Andersen, K. K.; Friis, S.; Majera, D.; Gursky, J.; Ozdian, T.; Bartkova, J.; Turi, Z.; Moudry, P.; Kraus, M.; Michalova, M.; Vaclavkova, J.; Dzubak, P.; Vrobel, I.; Pouckova, P.; Sedlacek, J.; Miklovicova, A.; Kutt, A.; Li, J.; Mattova, J.; Driessen, C.; Dou, Q. P.; Olsen, J.; Hajduch, M.; Cvek, B.; Deshaies, R. J.; Bartek, J. Alcohol-abuse drug disulfiram targets cancer via p97 segregase adaptor NPL4. *Nature* **2017,** 552, 194-199.

(28) Wang, L.; Bao, B. B.; Song, G. Q.; Chen, C.; Zhang, X. M.; Lu, W.; Wang, Z.; Cai, Y.; Li, S.; Fu, S.; Song, F. H.; Yang, H.; Wang, J. G. Discovery of unsymmetrical aromatic disulfides as novel inhibitors of SARS-CoV main protease: Chemical synthesis, biological evaluation, molecular docking and 3D-QSAR study. *Eur. J. Med. Chem.* **2017,** 137, 450-461.

(29) K., K.; Hallenbecka; David M. Turnera; Adam R. Rensloa; Arkina, M. R. Targeting Non-Catalytic Cysteine Residues Through Structure-Guided Drug Discovery. *Curr. Top. Med. Chem.* **2017,** 17, 4-15.

(30) Taylor, R. D.; MacCoss, M.; Lawson, A. D. Rings in drugs. *J. Med. Chem.* **2014,** 57, 5845-5859.

(31) Liu, Y.; Xie, Z.; Zhao, D.; Zhu, J.; Mao, F.; Tang, S.; Xu, H.; Luo, C.; Geng, M.; Huang, M.; Li, J. Development of the First Generation of Disulfide-Based Subtype-Selective and Potent Covalent Pyruvate Dehydrogenase Kinase 1 (PDK1) Inhibitors. *J. Med. Chem.* **2017,** 60, 2227-2244.

(32) Pietrucci, F.; Laio, A. A Collective Variable for the Efficient Exploration of Protein Beta-Sheet Structures: Application to SH3 and GB1. *J. Chem. Theory Comput.* **2009,** 5, 2197-2201.

(33) Lalau, J. D.; Race, J. M. Lactic acidosis in metformin-treated patients. Prognostic value of arterial lactate levels and plasma metformin concentrations. *Drug Saf.* **1999,** 20, 377-384.

(34) Han, X.; Huang, Y.; Zhang, R.; Xiao, S.; Zhu, S.; Qin, N.; Hong, Z.; Wei, L.; Feng, J.; Ren, Y.; Feng, L.; Wan, J. New insight into the binding modes of TNP-AMP to human liver fructose-1,6-bisphosphatase. *Spectrochim. Acta. A Mol. Biomol. Spectrosc.* **2016,** 165, 155-160.

(35) Kabsch, W. Xds. *Acta Crystallogr. D* **2010,** 66, 125-132.

(36) Winn, M. D.; Ballard, C. C.; Cowtan, K. D.; Dodson, E. J.; Emsley, P.; Evans, P. R.; Keegan, R. M.; Krissinel, E. B.; Leslie, A. G. W.; McCoy, A.; McNicholas, S. J.; Murshudov, G. N.; Pannu, N. S.; Potterton, E. A.; Powell, H. R.; Read, R. J.; Vagin, A.; Wilson, K. S. Overview of theCCP4 suite and current developments. *Acta Crystallogr. D* **2011,** 67, 235-242.

(37) Emsley, P.; Cowtan, K. Coot: model-building tools for molecular graphics. *Acta Crystallogr. D* **2004,** 60, 2126-2132.

(38) Adams, P. D.; Grosse-Kunstleve, R.; Hung, L.-W.; Ioerger, T. R.; Airlie J.McCoy; Moriarty, N.; Randy J. Read; James C. Sacchettini; K.Sauter, N.; Terwilliger, T. C. PHENIX: building new software for automated crystallographic structure determination. *Acta Crystallogr.* **2010,** 58, 1948-1954.

(39) Best, R. B.; Zhu, X.; Shim, J.; Lopes, P. E. M.; Mittal, J.; Feig, M.; MacKerell, A. D. Optimization of the Additive CHARMM All-Atom Protein Force Field Targeting Improved Sampling of the Backbone ϕ, ψ and Side-Chain $\chi1$ and $\chi2$ Dihedral Angles. *J. Chem. Theory Comput.* **2012,** 8, 3257-3273.

(40) Vanommeslaeghe, K.; Hatcher, E.; Acharya, C.; Kundu, S.; Zhong, S.; Shim, J.; Darian, E.; Guvench, O.; Lopes, P.; Vorobyov, I.; Mackerell, A. D., Jr. CHARMM general force field: A force field for drug-like molecules compatible with the CHARMM all-atom additive biological force fields. *J. Comput. Chem.* **2010,** 31, 671-690.

(41) Jorgensen, W. L.; Chandrasekhar, J.; Madura, J. D.; Impey, R. W.; Klein, M. L. Comparison of simple potential functions for simulating liquid water. *J. Chem. Phys.* **1983,** 79, 926-935.

(42) Hess, B.; Bekker, H.; Berendsen, H. J. C.; Fraaije, J. G. E. M. LINCS: A linear constraint solver for molecular simulations. *J. Comput. Chem.* **1997,** 18, 1463-1472.

(43) Darden, T.; York, D.; Pedersen, L. Particle mesh Ewald: An $N \cdot \log(N)$ method for Ewald sums in large systems. *J. Chem. Phys.* **1993,** 98, 10089-10092.

(44) Hess, B.; Kutzner, C.; van der Spoel, D.; Lindahl, E. GROMACS 4: Algorithms for Highly Efficient, Load-Balanced, and Scalable Molecular Simulation. *J. Chem. Theory Comput.* **2008,** 4, 435-447.

Graphical abstract